ENVIRONMENTAL RESEARCH
LETTERS

LETTER • OPEN ACCESS

Impact of cloud radiative forcing on tropical cyclone frequency and intensity through tuning the cloud ice-to-snow diameter threshold

To cite this article: Lujia Zhang *et al* 2025 *Environ. Res. Lett.* **20** 014027

IOP Publishing Environ. Res. Lett. 20 (2025) 014027 https://doi.org/10.1088/1748-9326/ad9b3c

ENVIRONMENTAL RESEARCH
LETTERS

OPEN ACCESS

RECEIVED
12 August 2024

REVISED
21 November 2024

ACCEPTED FOR PUBLICATION
6 December 2024

PUBLISHED
17 December 2024

LETTER

Impact of cloud radiative forcing on tropical cyclone frequency and intensity through tuning the cloud ice-to-snow diameter threshold

Lujia Zhang[1,2], **Yuanyuan Huang**[3], **Mengqian Lu**[1,*] and **Xiaoming Shi**[3,4,*]

[1] Department of Civil and Environmental Engineering, The Hong Kong University of Science and Technology, Hong Kong Special Administrative Region of China, People's Republic of China
[2] Individual Interdisciplinary Program (Earth, Ocean and Atmospheric Science), Interdisciplinary Program Office, The Hong Kong University of Science and Technology, Hong Kong Special Administrative Region of China, People's Republic of China
[3] Division of Environment and Sustainability, The Hong Kong University of Science and Technology, Hong Kong Special Administrative Region of China, People's Republic of China
[4] Center for Ocean Research in Hong Kong and Macau, Hong Kong University of Science and Technology, Hong Kong Special Administrative Region of China, People's Republic of China
[*] Authors to whom any correspondence should be addressed.

E-mail: cemlu@ust.hk and shixm@ust.hk

Keywords: tropical cyclone, cloud radiation, synoptic circulation, global warming

Supplementary material for this article is available online

Abstract

Cloud radiative effect (CRE) is crucial for the development of tropical cyclones (TCs). This study investigates the impact of cloud radiation on TC seeds and TCs in an aquaplanet model by tuning 'threshold diameter to convert cloud ice particles to snow' (DCS). With increased cloud cover associated with higher DCS, seed frequency decreases, but the greater intensity increase of seeds leads to a higher survival rate from seeds to TCs. The changes in large-scale circulation within the models are responsible for the reduced seed frequency. Higher DCS enhances equatorial cloud liquid and ice amounts, thereby intensifying radiation heating to the tropics. Increased radiation leads to more moisture and higher temperatures at high levels and increases the temperature gradient from the tropics to the subtropics, thereby intensifying the Hadley circulation. The resulting decrease in convective available potential energy and intensification of vertical wind shear act as inhibiting factors for seed genesis. Besides, the presence of more high-level clouds accumulates both longwave and shortwave heating, creating favorable thermal conditions for the circulation to develop at the mesoscale. This process supports the growth of seeds into mature TCs, resulting in higher survival rates from seeds to TCs. The findings on TCs and CRE in aquaplanet models could serve as a foundation and provide evidence for studies conducted in more complex environmental conditions.

1. Introduction

Tropical cyclones (TCs), widely acknowledged as among the most formidable and awe-inspiring natural phenomena, have gained increasing attention in the scientific community due to their potential response to global warming (Kossin 2018, Lu and Xiong 2019, Guzman and Jiang 2021, Studholme *et al* 2022, Feng *et al* 2023, Zhang *et al* 2023). However, the assessment of future changes in TC characteristics remains challenged, as evidenced by conflicting results regarding the potential increase or decrease in frequency from multiple studies (Knutson *et al* 2019, Lee *et al* 2020, Shan and Yu 2020, Emanuel 2021, Vecchi *et al* 2021). The heterogeneity of TC datasets and the intricate interplay of environmental factors that shape their formation and evolution make it imperative to investigate the effects of individual environmental processes on TCs (Lanzante 2019, Cha *et al* 2020, Chand *et al* 2022).

Cloud radiative effect (CRE), identified as the difference between the all-sky radiation flux and the clear-sky flux (Medeiros *et al* 2021), exerts strong influences on atmospheric systems at various temporal scales, including interannual phenomena such as ENSO, subseasonal systems like Madden–Julian Oscillation (MJO), and intraseasonal systems such as TCs (Crueger and Stevens 2015, Radel *et al* 2016, Middlemas *et al* 2019, Ruppert *et al* 2020, Medeiros *et al* 2021, Wu *et al* 2021). Clouds enveloping storms intercept the infrared radiation emitted by Earth's surface and lower atmosphere, inducing a localized warming of the lower-middle troposphere compared to the surrounding environment (Emanuel *et al* 2014, Wu *et al* 2021). This anomalous radiative heating further reinforces the circulation from the storm's inner core outward, thus augmenting clouds within the inner core. Ruppert *et al* (2019) proposed that the intensified circulation within the disturbance region facilitates the transport of increased moisture and low-level angular momentum, thereby enhancing the likelihood of TC development. This positive cloud radiation feedback (CRF) loop effectively accelerates the storm's gestation period and contributes significantly to its rapid intensification (Wing and Emanuel 2014, Wing *et al* 2016, Ruppert *et al* 2019). However, Yang *et al* (2022) recently introduced a novel perspective suggesting that CRF could induce a tilt in the eyewall of a TC, consequently constraining their capacity to attain higher intensities. Hence, there is a pressing need for investigations and explorations of the genesis and intensities of multiple TCs to better understand the thermodynamic and dynamic roles of CRE throughout the lifecycle of TCs.

Regional climate models (RCMs) like the Weather Research and Forecasting (WRF) model are widely undertaken to investigate the influence of CRE on TCs; however, due to the computational costs involved in accurately simulating TCs with high-resolution RCMs, prior studies mainly examined limited tropical depressions or TC tracks to explore the modulation of the CRE on cyclogenesis or intensity development (Ruppert *et al* 2019, Smith *et al* 2020, Yang *et al* 2021, 2022). Meanwhile, regional weather models primarily concentrate on the localized effects of cloud radiation while overlooking its broader influence on the global circulation patterns associated with climate change and the subsequent impacts on TC characteristics. General circulation models (GCMs) have demonstrated enhanced accuracy in simulating TC frequency, size, and structure since 2000 (Camargo and Wing 2016), due to advancements in tuning that enhance the representation of flow disturbances, temperature profiles, wind fields, and wave patterns (Li *et al* 2013, Hourdin *et al* 2017, Balaji *et al* 2022). Therefore, the utilization of GCMs is acknowledged as a credible and pioneering approach to explore the intricate interplay between CRE and TCs. By employing GCMs, we can investigate not only the influence of regional cloud radiation on TC development throughout its lifespan but also the modifications in global general circulation and the subsequent TC responses to diverse cloud processes.

As a category of GCM, idealized numerical model simulations on an aqua planet could serve as an insightful tool for investigating climate influences on TCs (Yoshioka and Kurihara 2008, Blackburn *et al* 2013, Merlis *et al* 2013, Williamson *et al* 2013). Regional perturbations like a warming pool on the ocean could be imposed to assess the potential impacts of regional climate features on TC behavior (Yoshioka and Kurihara 2008). Aquaplanet simulations also allow prescribed changes in key fields like SST profiles (Blackburn *et al* 2013, Williamson *et al* 2013), CO_2 levels, and cross-equatorial heat flux (Merlis *et al* 2013), to explore TC frequency and track responses to altered environmental conditions. However, the influence of changing CRE on TCs remains unexplored to the best of our knowledge. Therefore, we adopt the idealized aquaplanet framework for the GCM simulation to isolate the effects of cloud radiation on the physical processes governing the formation and evolution of TCs from terretrial influences. The aquaplanet configuration, characterized by the absence of land, vegetation, topography, and sea ice, and with only ocean-covered lower boundary conditions, serves as a valuable framework for a focused examination of the cloud radiation change on TCs by eliminating some external forcings and atmospheric variations. The following questions will be addressed:

(1) How do the characteristics of TC seeds and TCs change under different cloud conditions?
(2) What are the underlying large-scale environmental changes associated with different cloud radiative forcing that influence storm dynamics?
(3) What is the localized impact of different cloud radiative forcing on TCs?

To address these three questions, we perform the aquaplanet GCM simulations with varying 'threshold diameter to convert cloud ice particles to snow' (DCS), followed by TC detection and analysis within each experiment. Additionally, we analyze the changes in cloud properties under a warming scenario to gain insights into potential shifts in cloud radiation induced by climate change. The experimental design and methodology are detailed in section 2, followed by the examination of TC responses to cloud radiation and the underlying mechanisms in section 3. Finally, our conclusions and discussions are presented in section 4 and 5.

2. Model and methods

2.1. Aquaplanet model and experiment design

In our study, we utilize the Community Atmosphere Model version 6 (CAM6) within the Community Earth System Model version 2 (CESM2) to investigate the changes in TC characteristics. The CAM6 aquaplanet configuration involved running the model with zonally symmetric sea surface temperature (SST) prescribed above the default settings. The latitudinal structures of the SST field, termed 'Qobs' (Neale and Hoskins 2000), are close to the observed profile in the Pacific with a maximum of 300.15 K at the equator, decreasing to ∼60° latitude symmetrically (figure S1). The aquaplanet model employs a finite volume dynamical core with a horizontal resolution of 0.9° latitude × 1.25° longitude and includes 32 hybrid sigma-pressure levels. The Cloud Layers Unified by Binormals parameterization is utilized to represent boundary layer turbulence, shallow convection, and cloud macrophysics (Golaz *et al* 2002, Bogenschutz and Krueger 2013). The Rapid Radiative Transfer Model for General Circulation Models is employed for simulating radiative transfer processes (Iacono *et al* 2000), while the deep convection scheme follows Zhang and McFarlane (1995). The cloud microphysics scheme is from Gettelman and Morrison (2015), which incorporates a new representation of autoconversion to reduce sensitivity (Gettelman *et al* 2019). Additional details regarding the aquaplanet setup can be found in Medeiros *et al* (2016).

Among the 16 cloud microphysics and aerosol parameters in the Community Atmosphere Model-including the parameters such as the cloud droplet number limiter, minimum sub-grid vertical velocity for cloud droplet activation, and fall-speed parameters for cloud ice and snow- the cloud droplet size (DCS) has been identified as one of the most influential parameters affecting net radiative fluxes (Zhao *et al* 2013, Eidhammer *et al* 2014). DCS also exhibits strong sensitivity to other climate variables, such as precipitation rates and cloud amounts at mid and high levels, making it an effective parameter for investigating specific questions related to CRF (Pathak *et al* 2020, Fan *et al* 2021, Huang *et al* 2024). Increasing DCS reduces the efficiency of converting cloud ice to snow, resulting in a greater presence of cloud ice in the atmosphere and stronger CRF. To investigate the influence of DCS on CRE, we conduct three controlled experiments using the CAM6 aquaplanet model, varying the DCS values as 200 μm, 500 μm (default), and 800 μm. Each experiment is run for ten years, with the first two years discarded as spin-up, and the output data is archived daily. Figure S2(a) presents the precipitation snapshots on the first day after the model spin-up, and we could observe that some precipitation bands extend from the ITCZ and reach the midlatitude, resembling the atmospheric rivers in Earth's present-day climate, which are directly related to baroclinic waves (Zhang *et al* 2021b). Intense circular precipitation snapshots also exist in the tropics, which are potentially TCs that we aim to investigate. Besides, the tropical climate reaches an equilibrium between Day 730 and 3650 (figure S2(b)) after the initial spin-up, which we select as our study period.

Another warming experiment is modified based on the experiment with DCS setting to 500 μm to figure out the response of the cloud radiation with a more warming scenario. The SST is elevated by 5 K (SST + 5 K) and the CO2 concentration is quadrupled (4 × CO2). Henceforth, the experiments with DCS of 200 μm, 500 μm, and 800 μm, along with the warming experiment, will be referred to as Group_{200}, Group_{500}, $\text{Group}_{800,}$ and $\text{Group}_{\text{warming}}$, respectively, in the subsequent sections.

2.2. Seed and TC tracks definition

We distinguish between weak TC seeds and TCs identified as structured vortices to facilitate accurate detection and support further analysis. The detection is performed within the tropical region (30° S–30° N) to avoid the misdetection of the extratropical cyclones produced by the front system. Besides, within the equatorial region bounded by 5° S–5° N, where the Coriolis force is relatively weak for tropical cyclogenesis to occur, specific random cyclonic systems may manifest and form highly localized and short-lived storm tracks that remain confined within the equatorial region (Li *et al* 2013). Therefore, vortices originating within 5° of the equator are excluded to preserve the analytical integrity. To determine the seed tracks, we initially identify different vortices by connecting grids with 850 hPa relative vorticity (RV850) greater than 3.0×10^{-5} s^{-1} (taking the absolute value for grids in the southern hemisphere) and define the center of each vortex as the location with the minimum pressure among all the relevant grids (Ikehata and Satoh 2021). Subsequently, vortices with distances less than 10° between consecutive 1 d time steps are connected to form seed tracks, which are then considered for further analysis if they persist for a minimum of 3 d.

The TC tracking algorithm (henceforth tracker) used in this study is improved based on the open-source TempestExtremes tracker (Ullrich and Zarzycki 2017). Previous studies have proven the feasibility of utilizing the minimum surface pressure criterion to find TCs in aquaplanet models (Chavas *et al* 2017, Chavas and Reed 2019). The detailed procedures to find the TC tracks in the models are as follows:

1. Presence of the storm system: TCs are identified using more stringent criteria compared to the seeds. The storm is validated if the surface pressure exhibits a minimum increase of 2 hPa from the storm center within an angular radius of 5°

in any direction. The location with the minimum pressure is defined as the center of the storm. These storm points are considered indicative of the maturity phase within the lifetime of the final TC tracks.

2. TC point continuity: the initial process involves linking mature TC points in consecutive daily time slices, where the separation between their centers is within a great circle distance of 10°. Subsequent procedures only consider the case of at least two or more consecutive storms that follow the same track.
3. TC point backtrack: a backtracking procedure is performed from the initial point in the track obtained from step 2 to identify potential seeds that precede the mature storms, thus facilitating the acquisition of the development stage. Seeds that preserve a distance of less than 10° from the point at the previous timestep are connected iteratively until no seed satisfying the aforementioned requirements is identified. If multiple points satisfy the requirement, the one closest to the previous timestep is selected (Suzuki-Parker 2012, Wu and Duan 2023).
4. TC point forward track: starting from the final point in the track obtained from step 2, we initiate a forward tracking process for potential seeds after the mature storms. Seeds that remain within a distance of less than 10° and are closest to the point at the subsequent timestep are iteratively connected until no seed meets the specified criteria (Suzuki-Parker 2012, Wu and Duan 2023). Following the inclusion of both the development stage from the backtrack and the dissipation stage from the forward track, the final tracks lasting for a minimum duration of 3 d are chosen as the TC tracks.

Figure S3 illustrates an example of one detected TC track in Group_{500} utilizing the aforementioned tracker. The mature storm points have exhibited a well-organized cyclone structure. Through the backtracking procedure, the previous disturbance responsible for the formation of this TC is identified. Conversely, in the subsequent detection procedure, the dissipation stage of the TCs is also captured, providing the full lifetime of the TCs.

2.3. Calculation of environmental variables

In accordance with prior investigations (Fudeyasu *et al* 2020, Ikehata and Satoh 2021), the environmental conditions in which both TCs and seeds exist are determined by computing averages within a radial range of 0°–5° from their respective centers, thereby enabling a direct assessment of the influence of environmental fields. The abbreviations of the variables used in this study are listed in table S1 and elucidated within Text S1 for reference. Additionally, we adopt the the genesis potential index (GPI) to relate the occurrence of TCs to large-scale environmental conditions favorable for their formation (Cavicchia *et al* 2023). The GPI is calculated with the equation as follows (Emanuel and Nolan 2004):

$$\mathrm{GPI} = \left|10^5 AV_{850}\right|^{3/2} \left(\frac{RH_{700}}{50}\right) \left(\frac{PI}{70}\right)^3 \times (1 + 0.1\mathrm{VWS})^{-2}. \quad (1)$$

Where AV_{850} is the absolute vorticity at 850 hPa, $RH_{700}$is the relative humidity at 700 hPa and VWS is the vertical wind shear (VWS) between 200 and 850 hPa. PI is the potential intensity (PI), a parameter emblematic of the theoretical upper limit of TC intensity, determined by factors such as SST and the intricate thermodynamic structure of the local vertical atmosphere (Bister and Emanuel 2002, Vecchi and Soden 2007). In addition to this version of GPI, the dynamical GPI has recently emerged as a diagnostic tool for understanding TC behavior and associated dynamical features (Wang and Murakami 2020, Huang *et al* 2023). However, an investigation into fundamental thermal factors like low-level humidity is needed, which is why we adopt the version of GPI proposed by Emanuel and Nolan (2004) in this study.

3. Response of seeds and TCs to variations in cloud radiation

Two distinct latitudinal peaks were observed in the latitudinal distribution of TC frequency. Approximately half of the TCs are located around 10°, benefiting from comparatively high SST and abundant moisture energy available therein. The remaining half generates at relatively higher latitudes due to the higher Coriolis force for the vortices to generate, which is also demonstrated by the evidence that seeds located at higher latitudes exhibit stronger relative vorticity at 850 hPa (figure 1(b)). Similarly, the latitudinal distribution of seeds also exhibited two prominent peaks. Besides, the tropical oscillations at typical time scales in the intraseasonal periods, including the MJO, Kelvin Waves, Equatorial Rossby (ER) waves, and combined Mixed Rossby gravity waves and tropical depressions (MT), also significantly modulate the probability of cyclogenesis (Schreck *et al* 2011, 2012, Landu *et al* 2020). The latitudinal peak of the genesis of seed tracks during active ER, Kelvin, and MT waves at 5° and 20° signifies the contribution of these tropical waves to the formation of the seeds and TCs (text S2; figures S4 and S5).

As the DCS increases from 200 to 800 μm, the frequency of seeds gradually reduces, particularly conspicuous within the latitudinal range of 5°–15°. The intrinsic characteristics of the seeds, such as relatively elevated maximum sustained wind (MSW), diminished minimum sea level pressure (MSP), and expanded spatial area from Group_{800} to Group_{200},

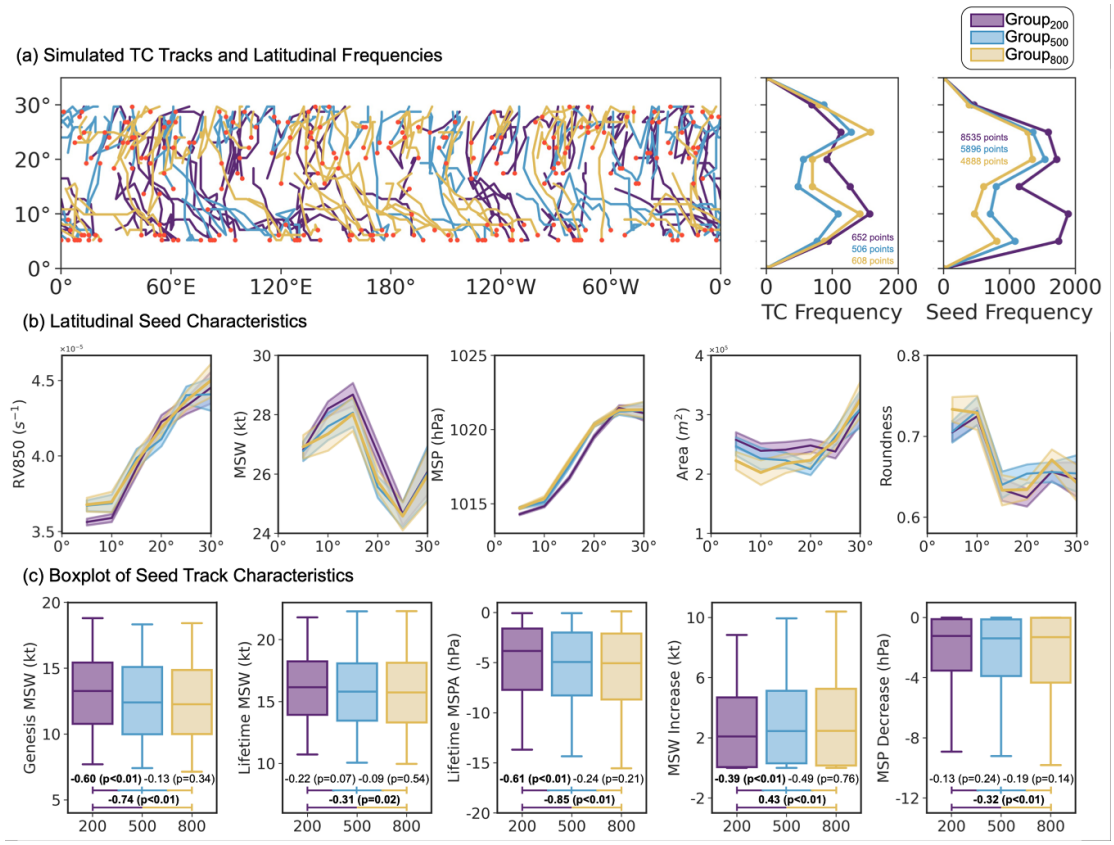

Figure 1. (a) Simulated TC tracks in three groups during the 8 year simulation period. The red dots are the genesis of the corresponding tracks. The latitudinal frequencies of TCs and seeds are depicted on the right side of the spatial tracks. The number is calculated as the sum within 5° latitudinal bins. The total number of TCs and seeds is also noted in the corresponding color. (b) Zonal mean of seed characteristics, including 850 hPa relative vorticity (RV850), maximum sustained wind (MSW), minimum sea level pressure (MSP), area, and roundness. The mean and 95% confidence levels are calculated using data points within 5° latitudinal bins. (c) Boxplots showing the characteristics in the seed tracks, including the MSW of the genesis, the lifetime maximum MSW during the seed tracks, the lifetime minimum MSP anomaly (MSPA) during the seed tracks, the maximum MSW increase during the seed tracks, and the minimum MSP decrease during the seed tracks. The MSPA is calculated as the difference between the MSP and the climatological MSP. The upper and bottom of the box are the 25 and 75 quantile values, while the upper and bottom of the whisker are the 5 and 95 quantile values. The differences in mean values between experiments are labeled with corresponding p-values (student t-test). Significant differences ($p < 0.05$) are labeled in bold font. The latitudes of samples in the Southern Hemisphere are taken as absolute values and combined with points in the Northern Hemisphere for calculation purposes.

once again underscore the enhanced viability for seed survival within Group_{200} (figure 1(b)). Because the TempestExtreme tracker necessitates a closed contour of 4 hPa within a certain distance, the roundness of the seeds can also determine the frequency of the detected TCs in different groups. Here we calculate the roundness as 4π times the area divided by the square of the perimeter (where a value of 1 signifies a perfect circle and declining towards 0 denotes markedly non-circular shapes). The roundness exhibits a substantial decrease from 10° to 15°, which can be attributed to the gradually intensified low-level wind, i.e. zonal wind at 850 hPa (U850; figure 2(e)). Consequently, the occurrence of detected TCs diminishes significantly at approximately 15° (figure 1(a)). However, the closely similar roundness values observed across these three groups suggest that the variation in shape does not appear to be the causal factor contributing to the observed disparities in frequency.

In contrast to the seed frequency, the detected TCs do not strictly conform to the fluctuations observed in seed counts. The results indicate a gradual increase in survival rates of 7.63%, 8.58%, and 12.49% from seeds to TCs that corresponded to stepwise enhancements in the DCS. Around 25° latitude, the TC count is already reversed, with Group_{800} showing the highest number and Group_{200} the lowest (figure 1(a)). Figure 1(c) provides statistical explanations for the enhancements in survival rates by illustrating the intensity characteristics linked to the seed tracks. Despite the decrease in both the mean of the genesis intensity and lifetime maximum intensity as DCS increases, the larger intensity growth indicators (MSW increase and MSP decrease) show a greater tendency for intensification within Group_{800} compared to Group_{200}. The 95th quantile of lifetime MSW and concomitantly 5th quantile of lifetime MSPA exhibit the strongest values within the high DCS group, thus substantiating the assertion that higher

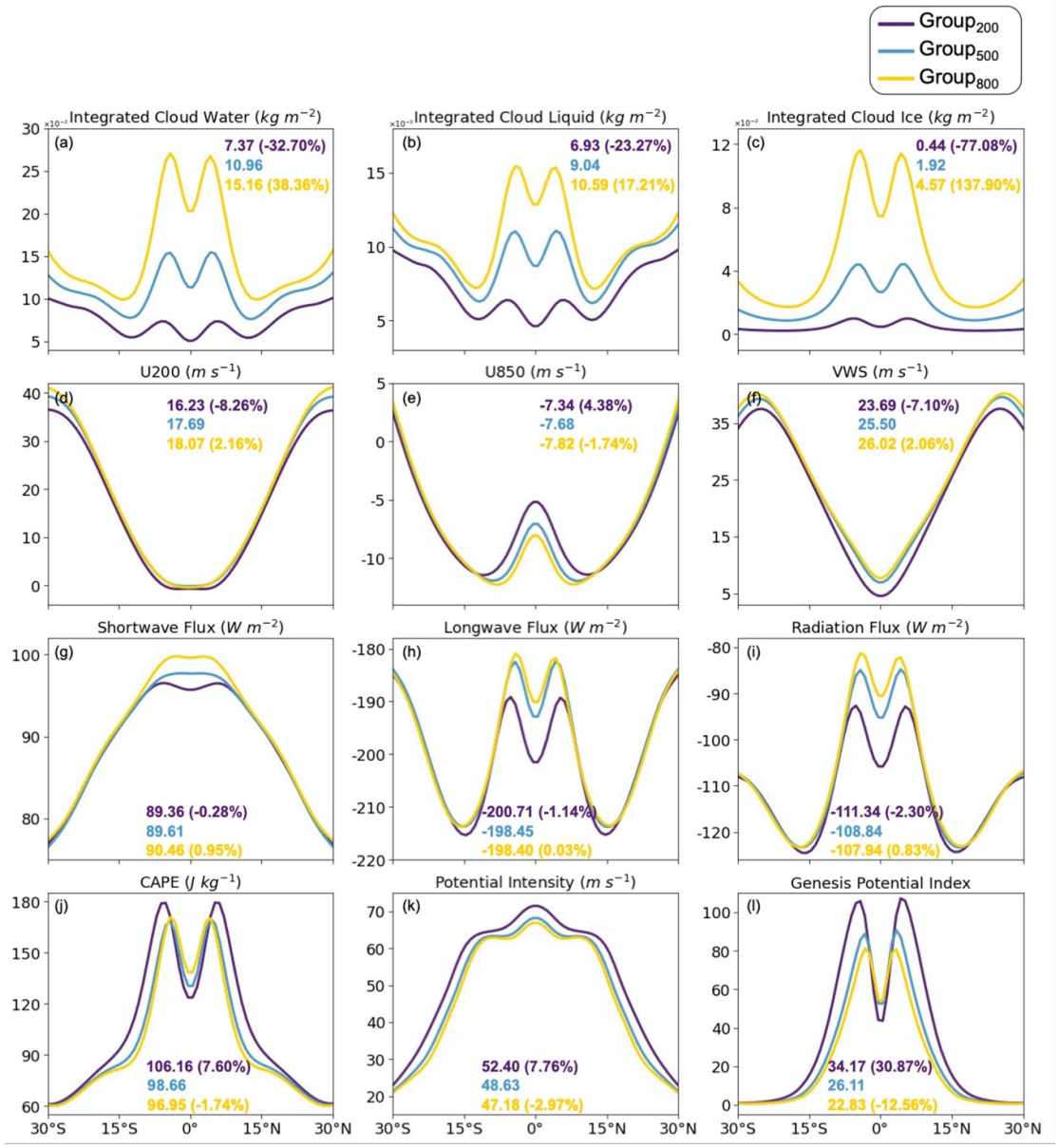

Figure 2. Climatology of zonal mean environmental fields across three groups from 30°S to 30°N, including (a) integrated cloud water (liquid and ice) across all layers, (b) integrated cloud liquid, (c) integrated cloud ice, (d) 200 hPa zonal wind (U200), (e) 850 hPa zonal wind (U850), (f) VWS, (g) shortwave flux convergence, (h) longwave flux convergence, (i) radiation flux convergence, (j) convective available potential energy (CAPE), (k) potential intensity, and (l) TC genesis potential index. The radiation flux convergence is calculated as the sum of the shortwave flux convergence and the longwave flux convergence. The flux convergence is calculated as the differences between top-of-model and surface net fluxes. The mean values for each group are noted in each subfigure. Percentage changes in $Group_{200}$ and $Group_{800}$ relative to the absolute value of $Group_{500}$ are also shown.

DCS is beneficial to the increase in TC intensity and engendering an elevated frequency of detected TCs. Therefore, with higher DCS values, the seeds generated around 20° are more likely to develop into TCs, resulting in a relatively higher number of TCs between 20° and 30°, as well as an overall higher seed-to-TC conversion ratio.

To further unveil the physical mechanisms underlying changes in the frequency of seeds, we investigate the environmental factors that impact the survival rate of the seeds (Ikehata and Satoh 2021). As DCS increases, there is a stepwise enhancement in cloud water content, encompassing both liquid and ice components, especially between latitudes 10°S and 10°N within the tropical region (figures 2 (a)–(c)). The abundant cloud could contribute to elevated radiation (including longwave and shortwave) flux (figures 2(g)–(i)), resulting in energy and moisture accumulation within the tropics and shown through higher temperatures and relative humidity at different levels (figures S7(a)–(d)). At latitudes higher than approximately 7°, the relatively drier and colder conditions at high altitudes in $Group_{200}$ lead to higher convective available potential energy

(CAPE; figures S7(b) and (d)), whereas at latitudes lower than 7°, the colder and drier conditions in the lower atmosphere counteract this effect, resulting in lower CAPE (figures S7(a) and (c)). Together, the CAPE is found to be 7.60% greater in $Group_{200}$ relative to $Group_{500}$ (figure 2 (j)), effectively contributing higher PI between 10° and 30° (figure 2(k)). Besides, a more pronounced energy gradient from the tropics to the subtropics (figure S7(a)) intensifies the Hadley circulation, as it is thermally driven (Bischoff and Schneider 2016, Huang *et al* 2024). The stronger Hadley circulation manifests as intensified westward U200 winds above 20° latitude and eastward U850 winds below 10° latitude (figures 2(d)) and (e)), which amplify the top-to-bottom wind difference at these locations, thereby enhancing the VWS and resulting in a 2.06% increase in $Group_{800}$ compared to $Group_{500}$ (figure 2(f)). The GPI calculated from the isolated variables highlights the positive contribution of higher AV850, higher PI, and lower VWS (figures S7(e), (g), and (h)), together yielding a substantial increase of 30.87% and a decrease of 12.56% in the GPI of $Group_{200}$ and Group800 compared to Group500 (figure 2(l)). The positive (negative) correlation of VWS (CAPE) with GPI across all seeds further substantiates their influence in generating fewer seeds with relatively higher cloud content (text S1; figure S6).

Instead of large-scale environmental influences, the storm-scale conditions during the developmental, mature, and dissipative stages of TCs could serve as the underlying mechanism for the positive relationship between survival rate and DCS. As depicted in figure 3(a), the rise of DCS acts as an obstacle to the ice-to-snow transformation, leading to a pronounced increase of high-level clouds, particularly during the development and maturity stages of TCs. This enrichment in high-level clouds in turn weakens the cooling effects of the longwave radiation due to the absorption of radiation energy in the mid-level cloud layers. The lower relative longwave cooling in $Group_{800}$ across all three stages indicates a more apparent reduction in radiation cooling effects due to the presence of clouds (figure 3(b)). The most notable difference is observed during the development stage, suggesting the onset of the warming effect attributed to cloud-induced absorption of longwave radiation at this stage. In $Group_{500}$, the formation of clouds is delayed compared to $Group_{800}$, which leads to the influence of clouds being more evident during the maturity stage rather than occurring concurrently as observed in $Group_{800}$. Besides, higher DCS leads to an intensified warming effect associated with shortwave radiation, primarily in high-level clouds with relatively lower energy magnitudes compared to longwave radiation (figure S8(a)), particularly obvious in $Group_{800}$ (figure S8(b)). Together, $Group_{800}$ receives the strongest radiative warming effect from 700 to 250 hPa during the development stage (figure S10(a)), thus fostering the enhancement of the thermally direct transverse circulation and facilitating efficient upward moisture transport (Yang *et al* 2021). Consequently, we observe an intensification of potential vorticity tendency (text S3; figure S9). The above results suggest that a higher DCS promotes the maintenance and development of deep convection, thereby facilitating the easier development of stronger TCs.

4. Summary

In this study, we explore the impact of CRE on the characteristics of TC seeds and TCs by modulating a pivotal cloud microphysics parameter, DCS, in the aquaplanet simulation. Higher DCS hinders the transformation of cloud ice to snow, thereby leading to an increased accumulation of clouds in the atmosphere. Accompanied by the presence of more clouds, the frequency of seeds decreases while the survival rate from seeds to TCs increases gradually among three groups of experiments. Figure 4 offers a graphical summary of the main mechanisms that happen with a higher DCS. We observe that more clouds accumulate in the upper atmosphere along the equatorial belt, resulting in increased radiation energy accumulation within the tropics. The greater increase in humidity and temperature at higher altitudes leads to a reduced CAPE distribution ranging from 5° to 30°. Besides, the amplified energy gradient from the tropical to subtropical latitude enhances the Hadley circulation, strengthening the low-level trade wind and producing stronger VWS in the simulation. Therefore, the probability of seed genesis is reduced, which arises from the adverse effects of weaker CAPE on vortex development and the disruptive influence of stronger VWS on the vertical structure of the vortex. Distinct from the large-scale effects, the intensified high-level cloud coverage creates favorable thermal conditions at the mesoscale, facilitating the development of seeds into TCs. The longwave cooling is reduced while the shortwave warming is intensified, collectively enhancing thermal conditions in the mid-to-high level region, thereby enhancing potential vorticity for vortices during the development stage. Vortices thereby gain the potential to reach higher intensities, consequently increasing the calculated survival rate from seeds to TCs in the aquaplanet simulation. In this idealized simulation, both the negative and positive effects of CRF on TCs are observed: the negative role of the general circulation primarily inhibits TC genesis, while the positive contribution of the radiation energy promotes the development of weak seeds into stronger TCs (Ruppert *et al* 2019, Yang *et al* 2022).

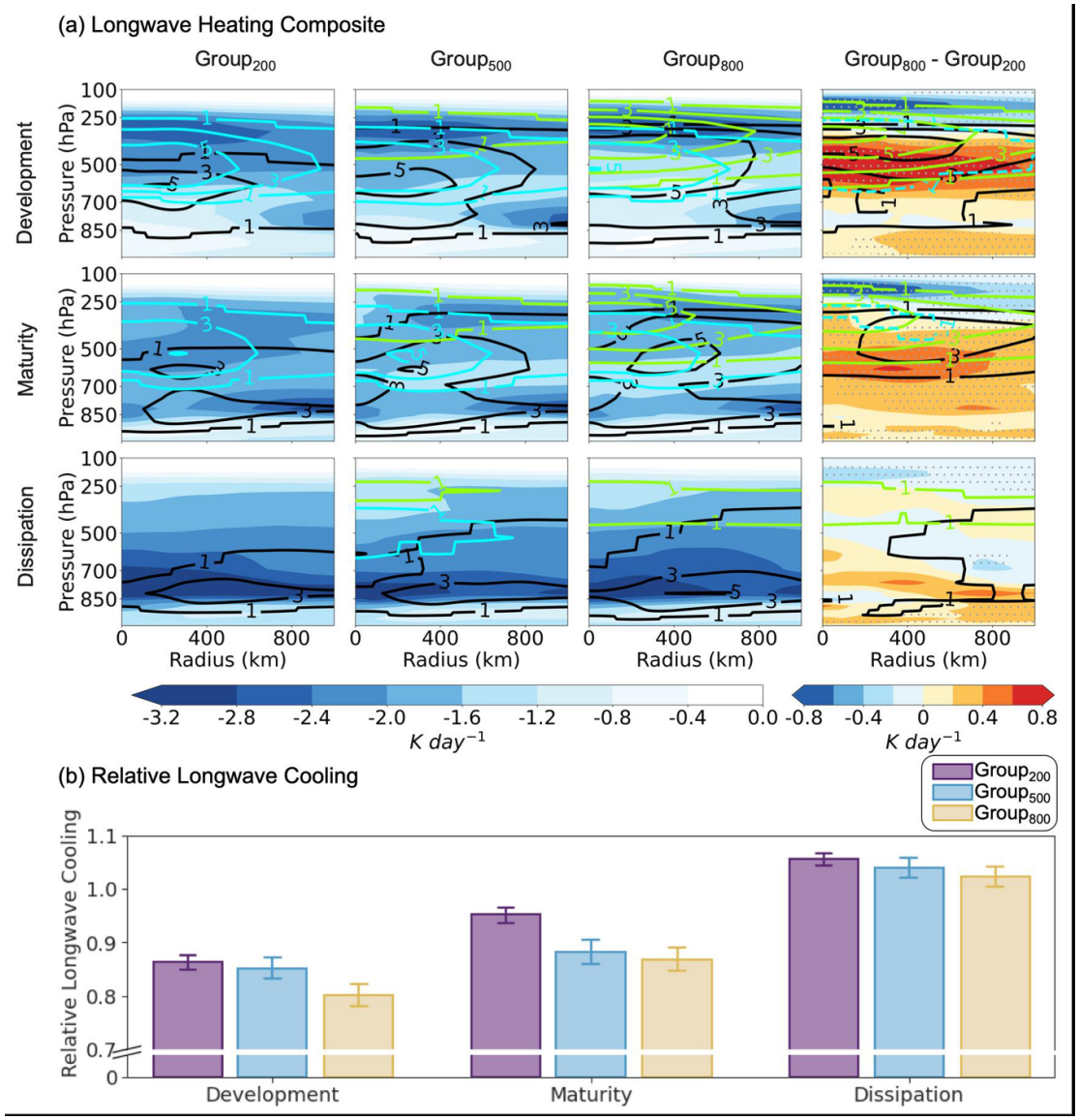

Figure 3. (a) Azimuthal mean of longwave heating rate (shading) of TCs. Columns 1–3 represent TCs in $Group_{200}$, $Group_{500}$, and $Group_{800}$, with green (cyan) contours indicating ice (snow) concentration ($\times 10^{-5}$ kg kg^{-1}). The black contours are the cloud fraction ($\times 10^{-5}$). The final column illustrates longwave heating rate differences between TCs in $Group_{800}$ and $Group_{200}$, with gray stippling indicating statistical significance at the 5% level (student t-test). Solid (dashed) lines represent positive (negative) differences in ice and snow concentrations ($\times 10^{-5}$ kg kg^{-1}) and cloud fraction ($\times 10^{-5}$). Rows from top to bottom represent TCs in the development, maturity, and dissipation stages. (b) Bar plots of the relative longwave cooling for TCs during three stages. The relative longwave cooling is calculated as the difference between the top-of-model and surface net longwave fluxes divided by the corresponding climatological values at the latitude of the TC. Black error bars denote the 95% confidence interval.

5. Discussion

Recent studies have noted an increasing frequency of intense TCs under global warming (Kossin *et al* 2020, Emanuel 2021). Another aquaplanet experiment named $Group_{warming}$, characterized by an SST + 5 K and 4 × CO2 setup compared to $Group_{500}$, displays an increased presence of climatological high-level clouds spanning from 15° to 30° (text S4; figure S11). More high-level clouds are induced by a reduction in the downward circulation due to the weakened Hadley circulation (text S4; figure S12). In the presence of such a climatological distribution, the detected TCs also contain more cloud ice and intensified radiation warming in the high-level vertical profile during the development stage (figure S13), potentially gaining the likelihood of attaining higher intensities. Furthermore, the energy accumulation resulting from the absorption of longwave radiation warms the atmosphere in the vertical profile. The similar changes in high-level cloud observed in $Group_{warming}$ and $Group_{800}$ suggest that cloud-related processes may partly contribute to the discovered increase in TC intensity and decrease in TC frequency (Elsner *et al* 2008, Chand *et al* 2022).

Owing to the inherent limitations in terms of computational and storage requirements, GCMs tend to have relatively coarse resolution compared to RCMs, which usually produce weaker and larger storms with less realistic dynamical structures

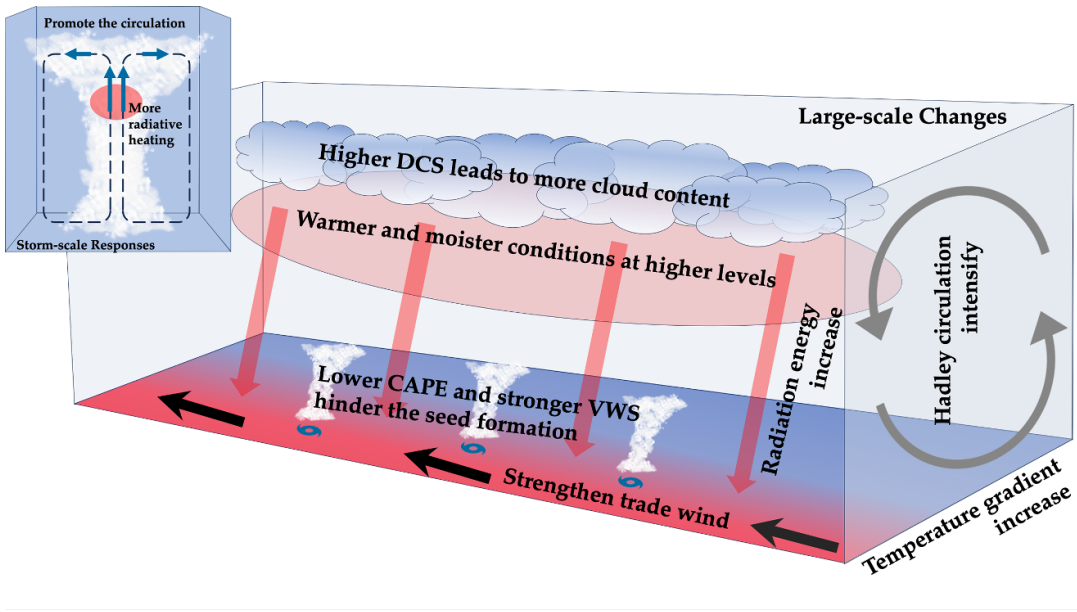

Figure 4. Schematic depicting the influence of higher DCS in the aquaplanet model. The rectangular box depicts changes in the large-scale environment. The red arrows denote the flow of radiation energy. The black arrows symbolize the trade winds. The curved gray arrows represent the Hadley circulation. The blue spirals and white cloud systems above represent TC seeds. The subfigure in the upper left depicts the response of TCs at the mesoscale. The red ellipse denotes the radiation. The blue arrows and the dashed lines depict the strengthened flow of the TCs.

(Camargo and Wing 2016, Roberts *et al* 2020, Faranda *et al* 2023). Despite employing the highest resolution settings in the CAM6 aquaplanet models, the radius of the localized TC feature surpasses those simulated in WRF and the inner core structures are not evident (Yang and Tan 2020). It is also important to acknowledge that change in the model resolution can alter climate feedbacks, such as the transition from positive to negative shortwave feedbacks observed with increasing resolution in the Icosahedral Non-hydrostatic model (Retsch *et al* 2019). These questions highlight the necessity for comprehensive research into the impact of resolution on CRF in future studies. Nevertheless, the basin and seasonal distributions of TCs in the latest CESM2 with the 0.9° latitude × 1.25° longitude resolution exhibit a close correspondence to observational results from 1980 to 2009 (figure S14). This consistency arises from the superior performance of CESM2 in simulating large-scale circulations and their variability, such as jet streams and stationary waves, which positions the CESM2 within the top 10% of the Coupled Model Intercomparison Project (Simpson *et al* 2020).

Moreover, the tracks of the detected TCs generated within the aquaplanet model exhibit some disparities compared to the real-world TCs, which do not follow the continuous paths originating from tropical easterly waves and subsequently propagating into the mid-latitudes (Li *et al* 2013). This disparity could potentially be attributed to the absence of some physical components within the aquaplanet configuration, such as the western North Pacific subtropical high. Besides, in comparison to the experimental setup featuring a single warming pool in the ocean, the presence of zonally symmetric SST conditions poses a hindrance to TCs to generate (Yoshioka and Kurihara 2008, Satoh *et al* 2015). Hence, in order to attain a more profound comprehension of the intricate processes governing realistic TCs and to elucidate disparities between observations and idealized model outputs, it becomes necessary to conduct a study that analyzes the intricate changes in TCs in response to CRF with a more realistic setup in the simulations. The present-day climate boundary conditions and altered radiation could be employed within the modeling framework to assess the effects on TCs (Zhang *et al* 2021a), which could be our forthcoming investigation.

Data availability statement

The CESM2 is obtained from www.cesm.ucar.edu/models/cesm2/. The data used to generate the figures in this study are available on Zenodo (Zhang and Huang 2024).

The data that support the findings of this study are openly available at the following URL/DOI: https://doi.org/10.5281/zenodo.10531237.

Acknowledgments

The work described in this paper was supported by Grants from the Research Grants Council (RGC) and National Science Foundation of China (NSFC). LJZ and ML are supported by the RGC funds (T22-501/23R & C6032-21G & YCRF C5002-22Y)

and NSFC-RGC fund (CRS_PolyU503/23). YYH and XS are substantially supported by RGC funds (AoE/P-601/23-N). XS is additionally supported by the RGC fund (HKUST-16307323 and AoE/E-603/18) and the Center for Ocean Research in Hong Kong and Macau (CORE), a joint research center between the Laoshan Laboratory and the Hong Kong University of Science and Technology (HKUST). The supercomputer Tianhe-2 used for computation is provided by the National Supercomputer Center in Guangzhou, China. We would like to extend our sincere appreciation to the two anonymous reviewers for their constructive and insightful comments, which played a crucial role in the improvement of this manuscript.

Conflict of interest

The authors declare that they have no known competing financial interests or personal relationships that could have appeared to influence the work reported in this paper.

ORCID iDs

Lujia Zhang https://orcid.org/0000-0001-7711-2383
Yuanyuan Huang https://orcid.org/0000-0003-4206-2632
Mengqian Lu https://orcid.org/0000-0002-8787-5621
Xiaoming Shi https://orcid.org/0000-0002-5329-7851

References

Balaji V, Couvreux F, Deshayes J, Gautrais J, Hourdin F and Rio C 2022 Are general circulation models obsolete? *Proc. Natl Acad. Sci. USA* **119** e2202075119
Bischoff T and Schneider T 2016 The equatorial energy balance, ITCZ position, and double-ITCZ bifurcations *J. Clim.* **29** 2997–3013
Bister M and Emanuel K A 2002 Low frequency variability of tropical cyclone potential intensity 2. climatology for 1982–1995 *J. Geophys. Res. Atmos.* **107** ACL-5
Blackburn M *et al* 2013 The aqua-planet experiment (APE): CONTROL SST simulation *J. Meteorol. Soc. Japan* **91** 17–56
Bogenschutz P A and Krueger S K 2013 A simplified PDF parameterization of subgrid-scale clouds and turbulence for cloud-resolving models *J. Adv. Model. Earth Syst.* **5** 195–211
Camargo S J and Wing A A 2016 Tropical cyclones in climate models *Wiley Interdiscip. Rev.* **7** 211–37
Cavicchia L, Scoccimarro E, Ascenso G, Castelletti A, Giuliani M and Gualdi S 2023 Tropical cyclone genesis potential indices in a new high-resolution climate models ensemble: limitations and way forward *Geophys. Res. Lett.* **50** e2023GL103001
Cha E J, Knutson T R, Lee T-C, Ying M and Nakaegawa T 2020 Third assessment on impacts of climate change on tropical cyclones in the Typhoon committee region—part ii: future projections *Trop. Cyclone Res. Rev.* **9** 75–86
Chand S S *et al* 2022 Declining tropical cyclone frequency under global warming *Nat. Clim. Change* **12** 655–61
Chavas D R and Reed K A 2019 Dynamical aquaplanet experiments with uniform thermal forcing: system dynamics and implications for tropical cyclone genesis and size *J. Atmos. Sci.* **76** 2257–74
Chavas D R, Reed K A and Knaff J A 2017 Physical understanding of the tropical cyclone wind-pressure relationship *Nat. Commun.* **8**
Crueger T and Stevens B 2015 The effect of atmospheric radiative heating by clouds on the madden-julian oscillation *J. Adv. Model. Earth Syst.* **7** 854–64
Eidhammer T, Morrison H, Bansemer A, Gettelman A and Heymsfield A J 2014 Comparison of ice cloud properties simulated by the community atmosphere model (CAM5) with *in-situ* observations *Atmos. Chem. Phys.* **14** 10103–18
Elsner J B, Kossin J P and Jagger T H 2008 The increasing intensity of the strongest tropical cyclones *Nature* **455** 92–95
Emanuel K 2021 Atlantic tropical cyclones downscaled from climate reanalyses show increasing activity over past 150 years *Nat. Commun.* **12** 7027
Emanuel K and Nolan D S 2004 Tropical cyclone activity and the global climate system *26th Conf. on Hurricanes and Tropical Meteorology*
Emanuel K, Wing A A and Vincent E M 2014 Radiative-convective instability *J. Adv. Model. Earth Syst.* **6** 75–90
Fan Y, Chung Y T and Shi X 2021 The essential role of cloud-radiation interaction in nonrotating convective self-aggregation *Geophys. Res. Lett.* **48** e2021GL095102
Faranda D, Messori G, Bourdin S, Vrac M, Thao S, Riboldi J, Fromang S and Yiou P 2023 Correcting biases in tropical cyclone intensities in low-resolution datasets using dynamical systems metrics *Clim. Dyn.* **61** 4393–09
Feng X, Yang G Y, Hodges K I and Methven J 2023 Equatorial waves as useful precursors to tropical cyclone occurrence and intensification *Nat. Commun.* **14** 511
Fudeyasu H *et al* 2020 Development conditions for tropical storms over the western north pacific stratified by large-scale flow patter *J. Meteorol. Soc. Japan* **98** 61–72
Gettelman A *et al* 2019 High climate sensitivity in the community earth system model version 2 (CESM2) *Geophys. Res. Lett.* **46** 8329–37
Gettelman A and Morrison H 2015 Advanced two-moment bulk microphysics for global models. Part I: off-line tests and comparison with other schemes *J. Clim.* **28** 1268–87
Golaz J C, Larson V E and Cotton W R 2002 A PDF-based model for boundary layer clouds. Part I: method and model description *J. Atmos. Sci.* **59** 3540–51
Guzman O and Jiang H 2021 Global increase in tropical cyclone rain rate *Nat. Commun.* **12** 5344
Hourdin F *et al* 2017 The art and science of climate model tuning *Bull. Am. Meteorol. Soc.* **98** 589–602
Huang X, Zhou T, Chan J C L, Zhan R, Chen Z and Zhao J 2023 Understanding uncertainties in projections of western North Pacific tropical cyclogenesis *Environ. Res. Lett.* **18** 114037
Huang Y, Kim D, Zhou T and Shi X 2024 The role of cloud-radiative interaction in tropical circulation and the Madden–Julian oscillation *J. Clim.* **37** 4559–76
Iacono M J, Mlawer E J, Clough S A and Morcrette J J 2000 Impact of an improved longwave radiation model, RRTM, on the energy budget and thermodynamic properties of the NCAR community climate model, CCM3 *J. Geophys. Res. Atmos.* **105** 14873–90
Ikehata K and Satoh M 2021 Climatology of tropical cyclone seed frequency and survival rate in tropical cyclones *Geophys. Res. Lett.* **48** e2021GL093626
Knutson T *et al* 2019 Tropical cyclones and climate change assessment: part i: detection and attribution *Bull. Am. Meteorol. Soc.* **100** 1987–2007
Kossin J P 2018 A global slowdown of tropical-cyclone translation speed *Nature* **558** 104–7
Kossin J P, Knapp K R, Olander T L and Velden C S 2020 Global increase in major tropical cyclone exceedance probability over the past four decades *Proc. Natl Acad. Sci. USA* **117** 11975–80
Landu K, Goyal R and Keshav B S 2020 Role of multiple equatorial waves on cyclogenesis over Bay of Bengal *Clim. Dyn.* **54** 2287–96

Lanzante J R 2019 Uncertainties in tropical-cyclone translation speed *Nature* **570** E6–E15
Lee T-C, Knutson T R, Nakaegawa T, Ying M and Cha E J 2020 Third assessment on impacts of climate change on tropical cyclones in the Typhoon committee region—part i: observed changes, detection and attribution *Trop. Cyclone Res. Rev.* **9** 1–22
Li F, Collins W D, Wehner M F and Leung L R 2013 Hurricanes in an aquaplanet world: implications of the impacts of external forcing and model horizontal resolution *J. Adv. Model. Earth Syst.* **5** 134–45
Lu M and Xiong R 2019 Spatiotemporal profiling of tropical cyclones genesis and favorable environmental conditions in the Western Pacific Basin *Geophys. Res. Lett.* **46** 11548–58
Medeiros B, Clement A C, Benedict J J and Zhang B 2021 Investigating the impact of cloud-radiative feedbacks on tropical precipitation extremes *npj Clim. Atmos. Sci.* **4** 18
Medeiros B, Williamson D L and Olson J G 2016 Reference aquaplanet climate in the community atmosphere model, version 5 *J. Adv. Model. Earth Syst.* **8** 406–24
Merlis T M, Zhao M and Held I M 2013 The sensitivity of hurricane frequency to ITCZ changes and radiatively forced warming in aquaplanet simulations *Geophys. Res. Lett.* **40** 4109–14
Middlemas E A, Clement A C, Medeiros B and Kirtman B 2019 Cloud radiative feedbacks and El Niño-Southern Oscillation *J. Clim.* **32** 4661–80
Neale R B and Hoskins B J 2000 A standard test for AGCMs including their physical parametrizations: i: the proposal *Atmos. Sci. Lett.* **1** 101–7
Pathak R, Sahany S and Mishra S K 2020 Uncertainty quantification based cloud parameterization sensitivity analysis in the NCAR community atmosphere model *Sci. Rep.* **10** 17499
Radel G, Mauritsen T, Stevens B, Dommenget D, Matei D, Bellomo K and Clement A 2016 Amplification of El Nino by cloud longwave coupling to atmospheric circulation *Nat. Geosci.* **9** 106–10
Retsch M H, Mauritsen T and Hohenegger C 2019 Climate change feedbacks in aquaplanet experiments with explicit and parametrized convection for horizontal resolutions of 2,525 Up to 5 km *J. Adv. Model. Earth Syst.* **11** 2070–88
Roberts M J *et al* 2020 Impact of model resolution on tropical cyclone simulation using the HighResMIP-PRIMAVERA multimodel ensemble *J. Clim.* **33** 2557–83
Ruppert J H, Wing A A, Tang X and Duran E L 2019 The critical role of cloud-infrared radiation feedback in tropical cyclone development *Proc. Natl Acad. Sci. USA* **117** 27884–92
Ruppert J H, Wing A A, Tang X and Duran E L 2020 Investigating the role of cloud-radiation interactions in subseasonal tropical disturbances *Geophys. Res. Lett.* **47**
Satoh M, Yamada Y, Sugi M, Kodama C and Noda A T 2015 Constraint on future change in global frequency of tropical cyclones due to global warming *J. Meteorol. Soc. Japan* **93** 489–500
Schreck C J, Molinari J and Aiyyer A 2012 A global view of equatorial waves and tropical cyclogenesis *Mon. Weather Rev.* **140** 774–88
Schreck C J, Molinari J and Mohr K I 2011 Attributing tropical cyclogenesis to equatorial waves in the western north pacific *J. Atmos. Sci.* **68** 195–209
Shan K and Yu X 2020 Interdecadal variability of tropical cyclone genesis frequency in western North Pacific and South Pacific ocean basins *Environ. Res. Lett.* **15** 64030
Simpson I R *et al* 2020 An evaluation of the large-scale atmospheric circulation and its variability in CESM2 and other CMIP models *J. Geophys. Res. Atmos.* **125** e2020JD032835
Smith W P, Nicholls M E and Pielke R A 2020 The role of radiation in accelerating tropical cyclogenesis in idealized simulations *J. Atmos. Sci.* **77** 1261–77
Studholme J, Fedorov A V, Gulev S K, Emanuel K and Hodges K 2022 Poleward expansion of tropical cyclone latitudes in warming climates *Nat. Geosci.* **15** 14–28
Suzuki-Parker A 2012 Tropical cyclone detection and tracking method *An Assessment of Uncertainties and Limitations in Simulating Tropical Cyclone Climatology and Future* (Springer Berlin Heidelberg) pp 9–26
Ullrich P A and Zarzycki C M 2017 TempestExtremes: a framework for scale-insensitive pointwise feature tracking on unstructured grids *Geosci. Model Dev.* **10** 1069–90
Vecchi G A, Landsea C, Zhang W, Villarini G and Knutson T 2021 Changes in Atlantic major hurricane frequency since the late-19th century *Nat. Commun.* **12** 4054
Vecchi G A and Soden B J 2007 Effect of remote sea surface temperature change on tropical cyclone potential intensity *Nature* **450** 1066–70
Wang B and Murakami H 2020 Dynamic genesis potential index for diagnosing present-day and future global tropical cyclone genesis *Environ. Res. Lett.* **15** 114008
Williamson D L *et al* 2013 The aqua-planet experiment (APE): response to changed meridional SST profile *J. Meteorol. Soc. Japan* **91** 57–89
Wing A A, Camargo S J and Sobel A H 2016 Role of radiative-convective feedbacks in spontaneous tropical cyclogenesis in idealized numerical simulations *J. Atmos. Sci.* **73** 2633–42
Wing A A and Emanuel K A 2014 Physical mechanisms controlling self-aggregation of convection in idealized numerical modeling simulations *J. Adv. Model. Earth Syst.* **6** 59–74
Wu S N, Soden B J and Nolan D S 2021 Examining the role of cloud radiative interactions in tropical cyclone development using satellite measurements and WRF simulations *Geophys. Res. Lett.* **48** e2021GL093259
Wu T and Duan Z 2023 A new and efficient method for tropical cyclone detection and tracking in gridded datasets *Weather Clim. Extremes* **42** 100626
Yang B, Guo X, Gu J F and Nie J 2022 Cloud-radiation feedback prevents tropical cyclones from reaching higher intensities *Geophys. Res. Lett.* **49** e2022GL100067
Yang B, Nie J and Tan Z M 2021 Radiation feedback accelerates the formation of Typhoon Haiyan (2013): the critical role of mid-level circulation *Geophys. Res. Lett.* **48** e2021GL094168
Yang B and Tan Z M 2020 Interactive radiation accelerates the intensification of the midlevel vortex for tropical cyclogenesis *J. Atmos. Sci.* **77** 4051–65
Yoshioka M K and Kurihara Y 2008 Influence of the equatorial warm water pool on the tropical cyclogenesis: an aqua plante experiment *Atmos. Sci. Lett.* **9** 248–54
Zhang B, Soden B J, Vecchi G A and Yang W 2021a The role of radiative interactions in tropical cyclone development under realistic boundary conditions *J. Clim.* **34** 2079–91
Zhang G J and McFarlane N A 1995 Sensitivity of climate simulations to the parameterization of cumulus convection in the canadian climate centre general circulation model *Atmosphere—Ocean* **33** 407–46
Zhang G, Silvers L G, Zhao M and Knutson T R 2021b Idealized aquaplanet simulations of tropical cyclone activity: significance of temperature gradients, hadley circulation, and zonal asymmetry *J. Atmos. Sci.* **78** 877–902
Zhang L, Cheng T F, Lu M, Xiong R and Gan J 2023 Tropical cyclone stalling shifts northward and brings increasing flood risks to East Asian Coast *Geophys. Res. Lett.* **50** e2022GL102509
Zhang L and Huang Y 2024 Dataset for the study "How do tropical cyclone frequency and intensity respond to more clouds? *Zenodo* (https://doi.org/10.5281/zenodo.10531237)
Zhao C *et al* 2013 A sensitivity study of radiative fluxes at the top of atmosphere to cloud-microphysics and aerosol parameters in the community atmosphere model CAM5 *Atmos. Chem. Phys.* **13**